

Supplementary Material

Interseismic coupling, megathrust earthquakes and seismic swarms along the Chilean subduction zone (38°-18°S)

1 GPS data set

We combined in a single data set the interseismic velocities published in Métois et al. [2013, 2014], together with the recent bolivian velocities from Brooks et al. [2011] and older data sets from SAGA [Khazaradze and Klotz, 2003], CAP [Brooks et al., 2003] and IPG teams [Ruegg et al., 2009] that we rotated in the ITRF 2008 reference frame following the method described in Métois et al. [2012]. Finally we rotated these velocities in the fixed South-America reference frame by applying the absolute SOAM rotation pole determined by NNR-Nuvel1A. We added to this horizontal velocity-field 72 GPS vertical displacements used by Métois et al. [2014] for the central Chile area and 27 others from Ruegg et al. [2009] already used by Métois et al. [2012], and included these 99 independent observations in the inversion procedure with a decrease weight (see supplementary figure 1).

2 Models resolution

The main issue in retrieving the coupling coefficient in subduction zones with respect to continental active faults is the lack of data in the vicinity of the trench, i.e. over the first kilometers depth of the fault interface. Furthermore, we sample the deformation on the upper plate only. In order to assess the resolution of our models, we follow Loveless and Meade [2011] and calculate the sensitivity of our network to each unit slip dislocation on the plate interface, or the power P of the network to resolve this unit slip (see supplementary figure 2). Our network is unable to resolve coupling on the first 10 km depth of the interface, except offshore the Tongoy peninsula where we should be able to discriminate between full or null coupling even in the shallowest nodes. We show alternative models in which the shallowest part of the trench is forced to be fully creeping or fully locked in supplementary figure 8 that demonstrate that our network is not sensitive to coupling from the trench to ~ 10 km depth. Obviously, the resolution is low at the edges of the model and in the scarcely instrumented Taltal area (25°-26°S). Overall, our network is sufficiently dense to resolve the coupling pattern between 10 and 45 km depth.

We also provide standard checkerboard tests in supplementary figure 3 that show the capability of the network to capture large (50 x 50 km) and small (25 km x 25 km) scales in the coupling distribution. While large scale variations of the coupling are well retrieved over almost all the subduction plane, smaller variations are only captured by the network in the 10 to 45 km depth range.

33 **3 Sliver rotation**

34 Alternative models using different smoothing constrains and plates configuration are presented in
35 supplementary figures 6 and 7. All of them present very similar along-trench variations in the coupling
36 coefficient (supplementary fig.5) but often exhibits significant differences in the along-dip amount of
37 coupling. We used coupling distributions that reproduce the data set with a lower than 2 nRMS to
38 plot the average coupling lateral variations in figure 3B of the main text (red dashed lines). In the
39 3-plate configuration, we inverted simultaneously for the coupling coefficient and the rotation pole of
40 an Andean sliver.

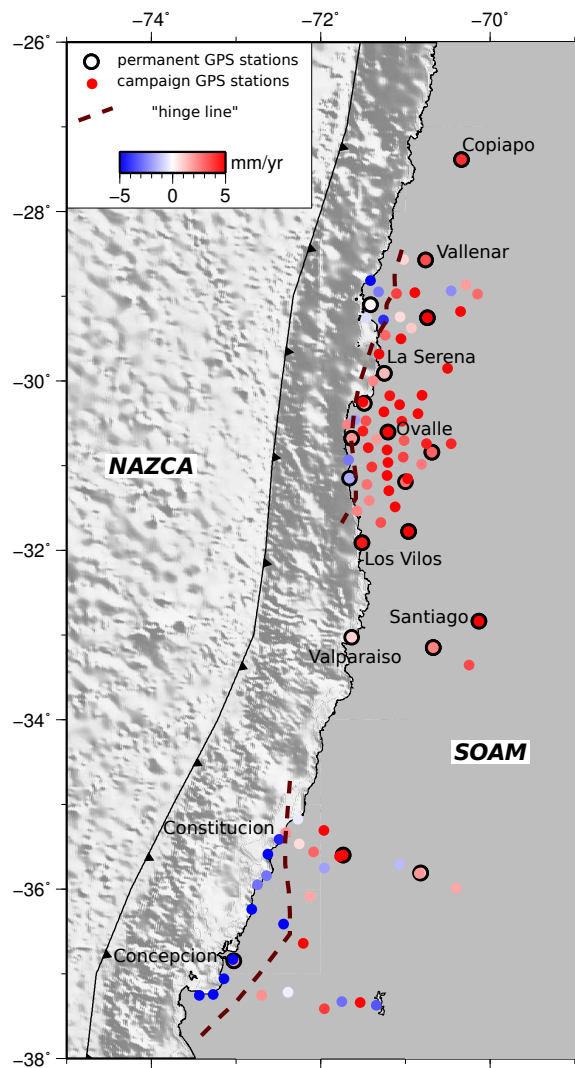


Fig.S 1: Combined vertical velocity field from continuous and campaign GPS measurements from [Ruegg et al., 2009, Métois et al., 2014]. Dashed brown line : supposed position of the hinge line.

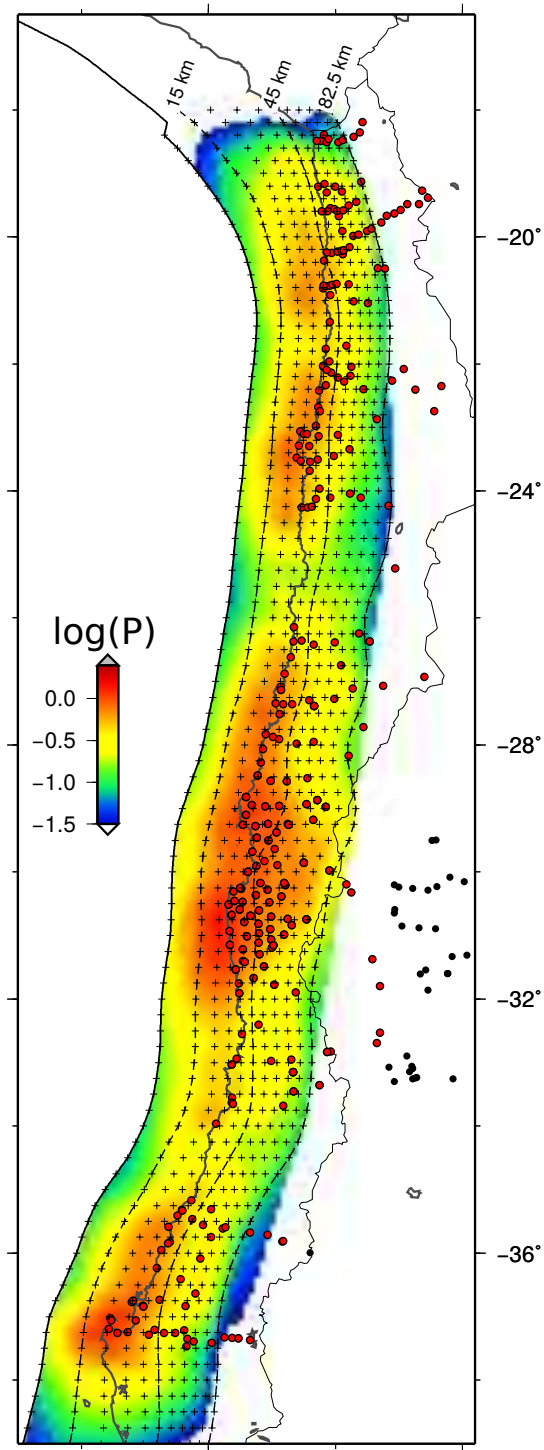


Fig.S 2: Sensitivity of horizontal data to unit coupling on the slab. Each element of the interface is colored by the log of the sum of the displacements (P in mm/yr) at GPS stations (dots) due to unit slip on the nearest grid node. Black crosses are slab nodes projection at surface.

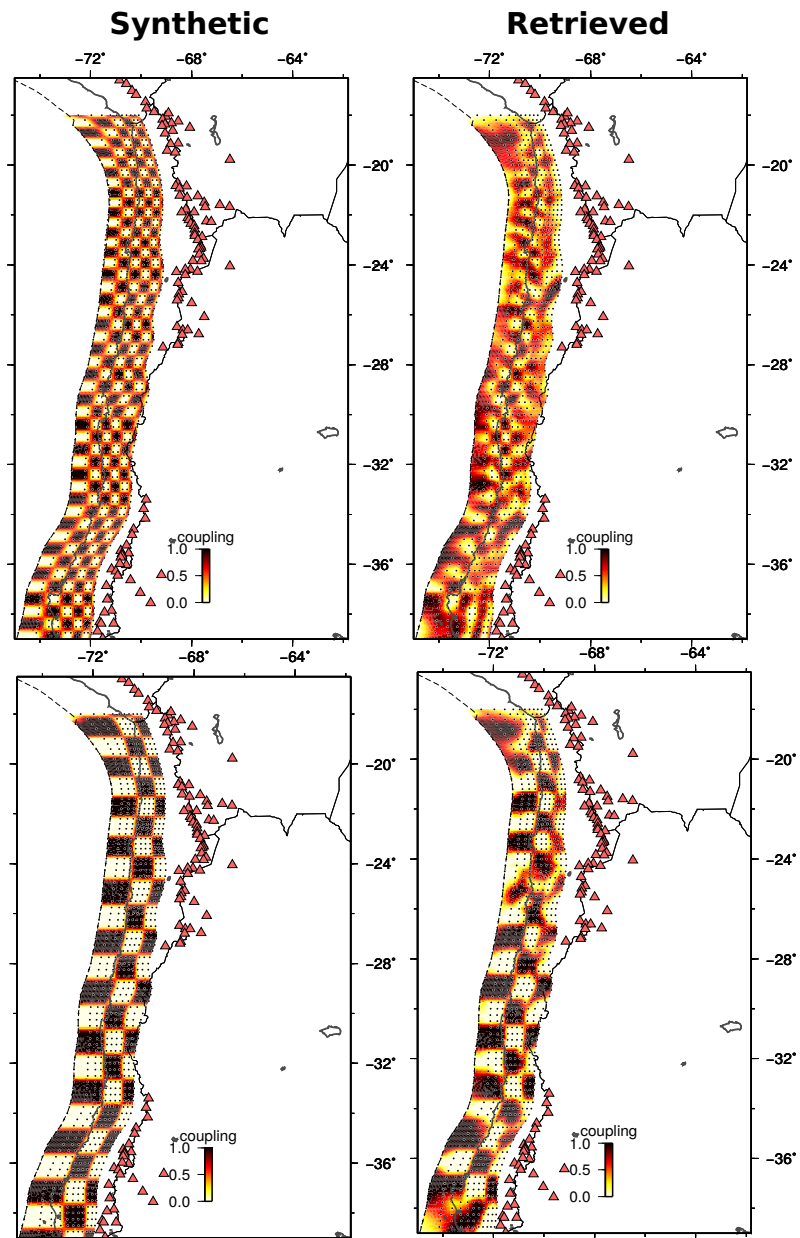


Fig.S 3: Checkerboard resolution tests. Left : synthetic checkerboard coupling distributions showing small scale (top, 25 x 25 km) or large scale (bottom 50 x 50 km) checkers. Right : coupling distribution inverted using the synthetic velocities.

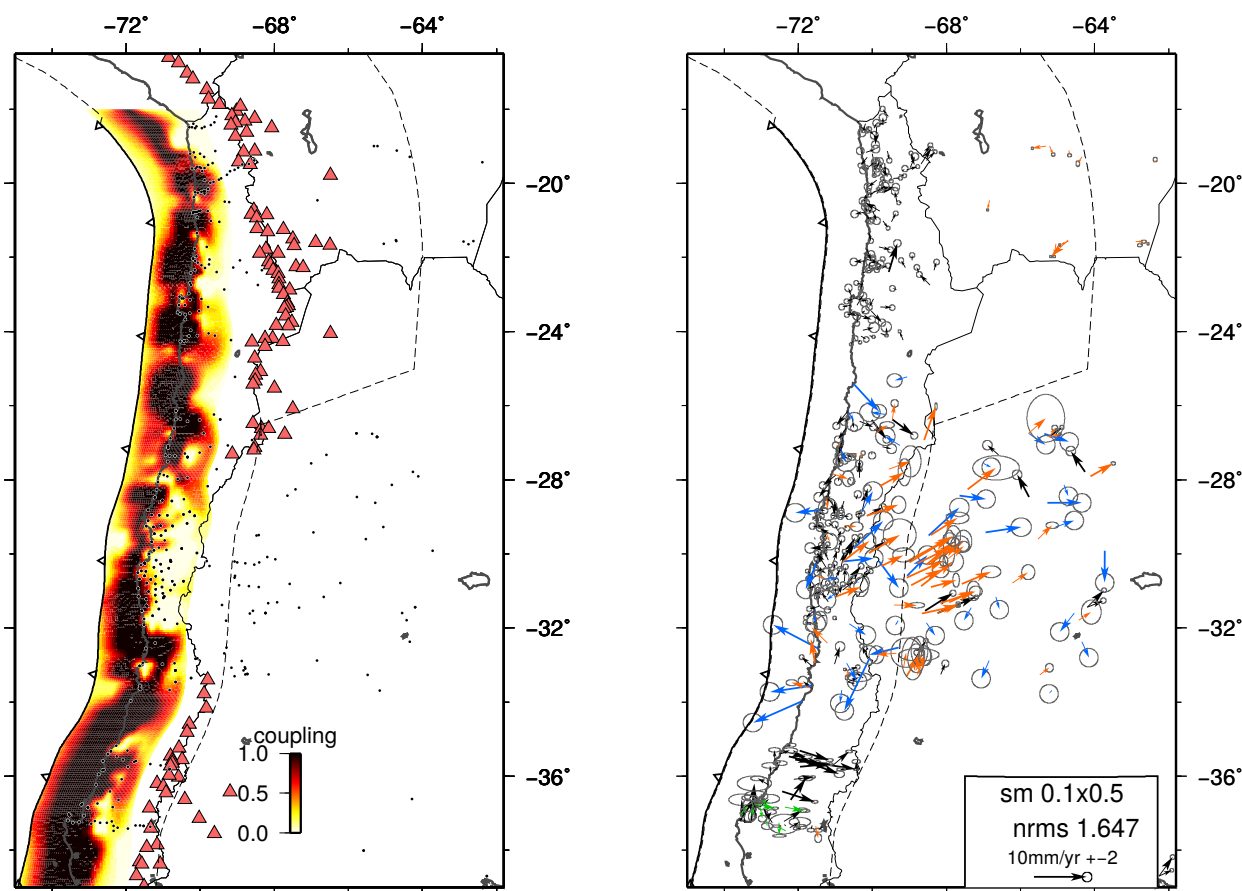


Fig.S 4: Best coupling model presented in figure 3 of the main text (left) and associated residuals (right) color-coded depending on the original data-set.

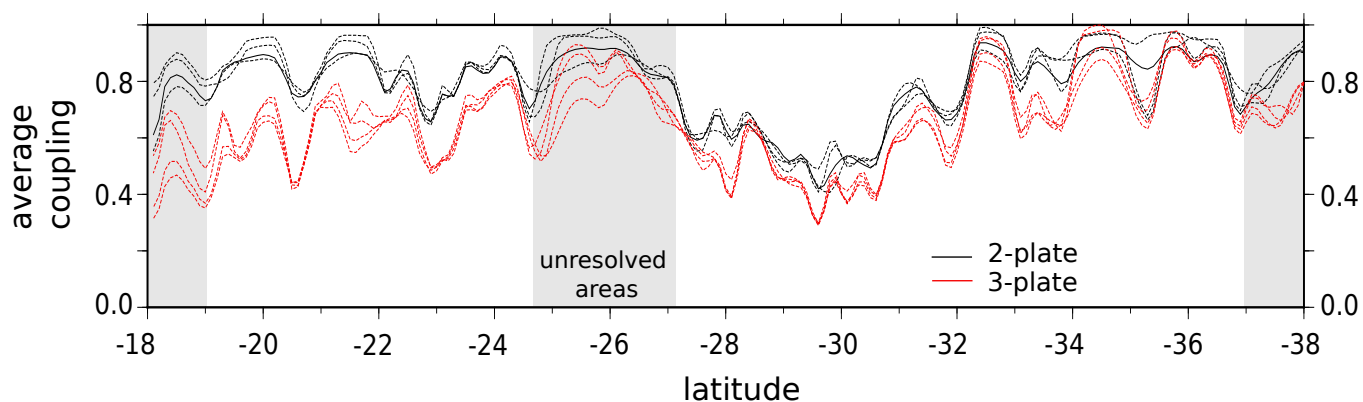


Fig.S 5: Along-strike variations of the averaged coupling value on the first 60 km depth of the slab for 2-plate (black curves) and 3-plate (red curves) models. Each curve corresponds to a distinct along-dip smoothing value. Gray shaded areas are areas lacking resolution (see supplementary Figs.2 and 3). Overall, small scale variations in the average coupling amount are very similar between 2- and 3-plate models. However, at larger scale, we interpret the lower average coupling value observed North of 30°S in the 3-plate models with respect to the 2-plate models as a consequence of the increasing Andean sliver motion going North. Therefore, we think this change in average coupling is an artifact of our modeling trick to retrieve the Andes kinematics rather than a real feature.

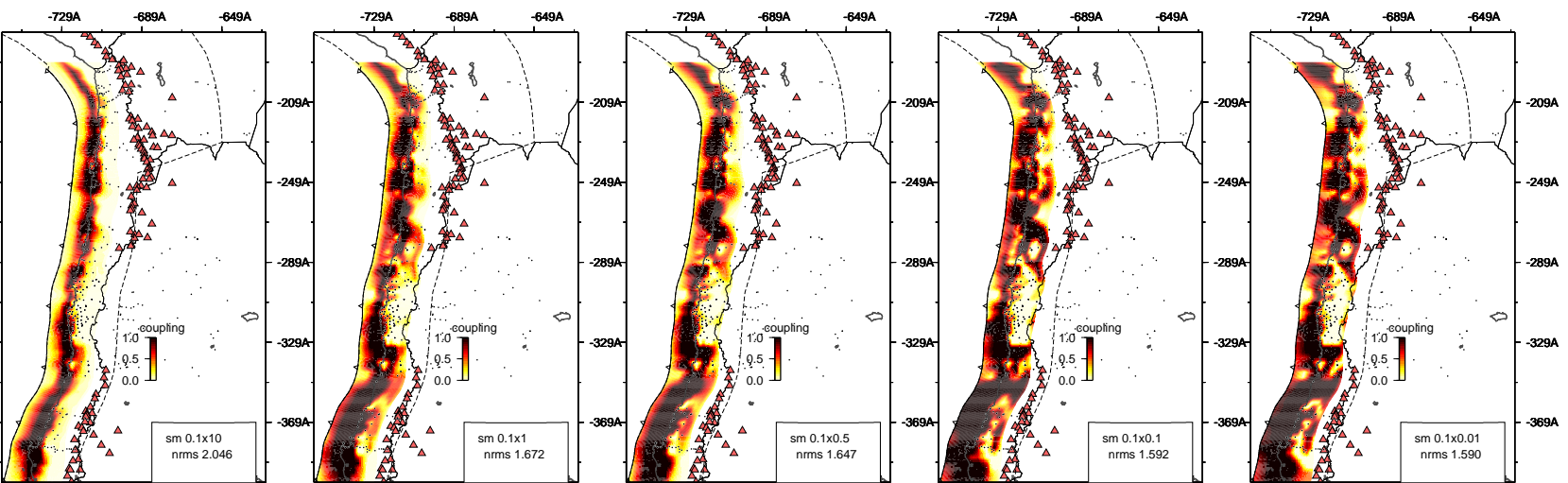


Fig. S.6: **3-Plate model / varying smoothing values** Coupling patterns inverted using different initial smoothing values simultaneously with the Andean sliver motion. Coupling is color coded as in main-text Figure 3. The smoothing value and the normalized root mean square are indicated in the bottom left corner of each plot.

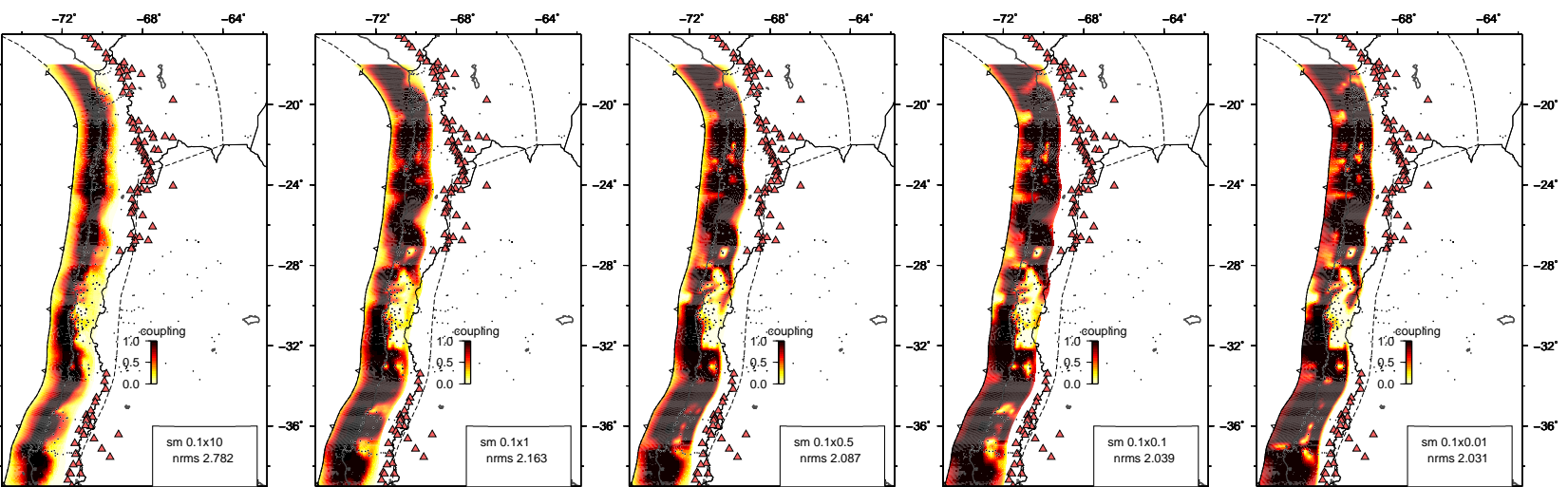


Fig. S 7: **2-Plate model / varying smoothing values** Same as supplementary figure 6 but for 2-plate configuration models, i.e. without Andean sliver motion.

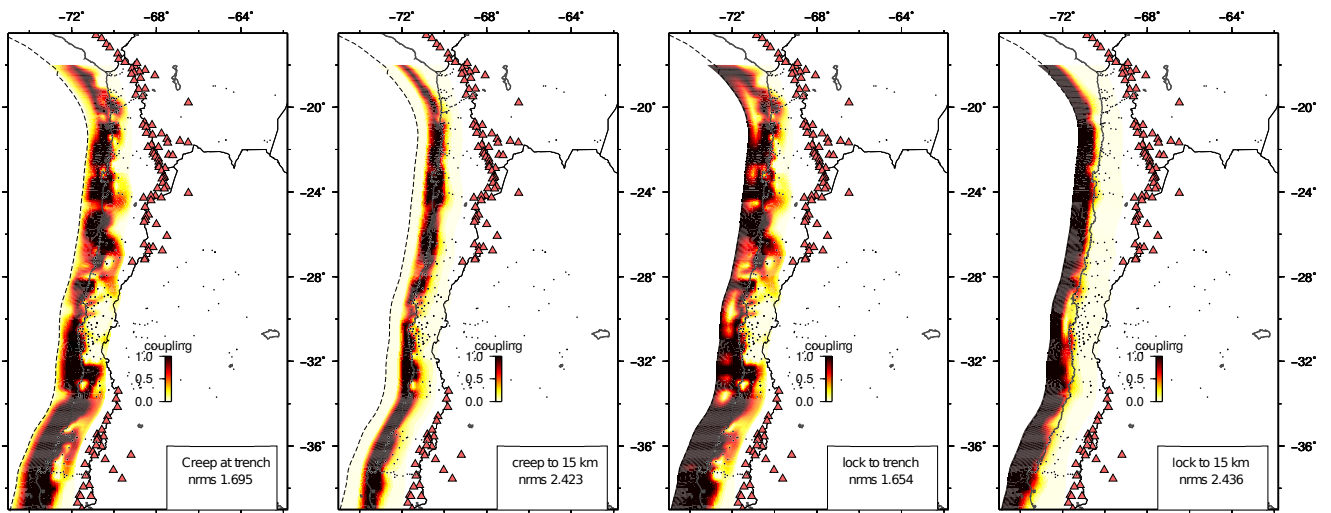


Fig.S 8: **3-Plate models / varying constraints on shallow nodes.** Same caption as supplementary figure 6 but with 0% or 100% coupling imposed on the shallowest nodes (7.5 km depth) or down to 15 km depth.

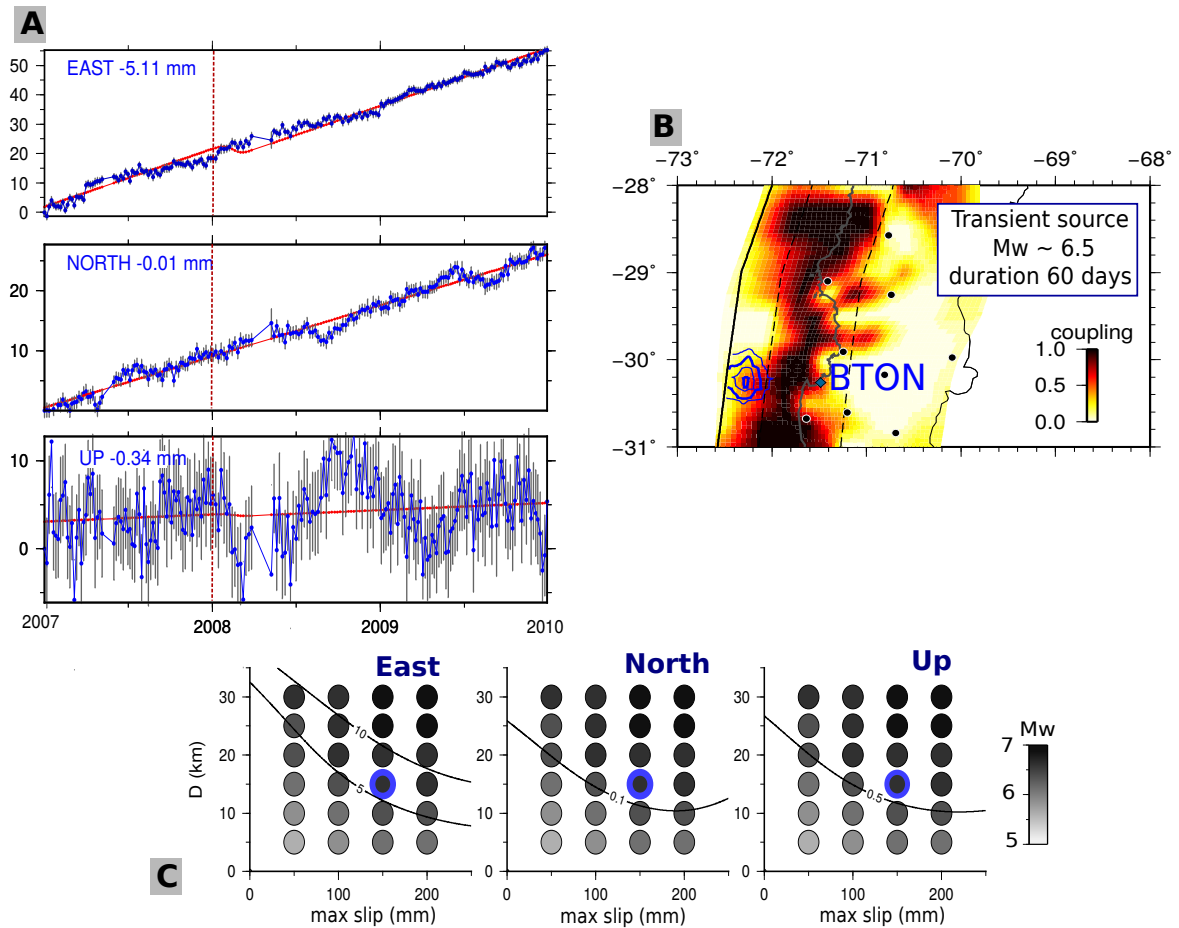


Fig.S 9: A- East, North and Up displacements of the continuous GPS station BTON (located in B) observed (blue dots) and predicted (red line) by an elastic model in which interseismic coupling is equivalent to the one presented in figure 3 of the main text, and a simulated slow slip event occur in 2008. Offsets produced by such an event are indicated in the upper left corner of each plot. B- 50 cm contours of this simulated SSE (blue lines) and network of continuous GPS stations (squares). Interseismic coupling is color coded. C- black lines : contours for 5, 10, 0.1 and 0.5 mm offsets produced at BTON depending on the size (D) and maximum amplitude of the SSE. SSE magnitude is color-coded. Blue-contoured dot: SSE model used for upper figures.

41 **References**

- 42 B.A. Brooks, M. Bevis, R. Smalley Jr, E. Kendrick, R. Manceda, E. Lauría, R. Maturana, and
43 M. Araujo. Crustal motion in the Southern Andes (26–36 S): Do the Andes behave like a mi-
44 croplate? *Geochemistry Geophysics Geosystems*, 4(10):1085, 2003. ISSN 1525-2027.
- 45 B.A. Brooks, M. Bevis, K. Whipple, J.R. Arrowsmith, J. Foster, T. Zapata, E. Kendrick, E. Minaya,
46 A. Echalar, M. Blanco, et al. Orogenic-wedge deformation and potential for great earthquakes in
47 the central andean backarc. *Nature Geoscience*, 4(6):380–383, 2011.
- 48 G. Khazaradze and J. Klotz. Short-and long-term effects of GPS measured crustal deformation rates
49 along the south central Andes. *Journal of geophysical research*, 108(B6):2289, 2003. ISSN 0148-
50 0227.
- 51 J.P. Loveless and B.J. Meade. Spatial correlation of interseismic coupling and coseismic rupture extent
52 of the 2011 mw9.0 tohoku-oki earthquake. *Geophys. Res. Lett*, 38:L17306, 2011.
- 53 M. Métois, A. Socquet, and C. Vigny. Interseismic coupling, segmentation and mechanical behavior
54 of the central chile subduction zone. *Journal of Geophysical Research*, 117(B3), 2012.
- 55 M. Métois, A. Socquet, C. Vigny, D. Carrizo, S. Peyrat, A. Delorme, E. Maureira, M-C. Valderas-
56 Bermejo, and I. Ortega. Revisiting the north chile seismic gap segmentation using gps-derived
57 interseismic coupling. *Geophysical Journal International*, 194(3):1283–1294, 2013.
- 58 M Métois, C Vigny, A Socquet, A Delorme, S Morvan, I Ortega, and C-M Valderas-Bermejo. Gps-
59 derived interseismic coupling on the subduction and seismic hazards in the atacama region, chile.
60 *Geophysical Journal International*, 196(2):644–655, 2014.
- 61 JC Ruegg, A. Rudloff, C. Vigny, R. Madariaga, JB De Chabalier, J. Campos, E. Kausel, S. Barrientos,
62 and D. Dimitrov. Interseismic strain accumulation measured by GPS in the seismic gap between
63 Constitución and Concepción in Chile. *Physics of the Earth and planetary interiors*, 175(1-2):
64 78–85, 2009. ISSN 0031-9201.